The Astrophysical Journal Letters, 793:L35 (7pp), 2014 October 1 doi:10.1088/2041-8205/793/2/L35

INTERACTION BETWEEN TWO CORONAL MASS EJECTIONS IN THE 2013 MAY 22 LARGE SOLAR ENERGETIC PARTICLE EVENT

Liu-Guan Ding[1,2], Gang Li[2], Yong Jiang[3], Gui-Ming Le[4], Cheng-Long Shen[5], Yu-Ming Wang[5], Yao Chen[6], Fei Xu[1], Bin Gu[1], and Ya-Nan Zhang[1]

[1] School of Physics and Optoelectronic Engineering, Institute of Space Weather, Nanjing University of Information Science and Technology, Nanjing 210044, China
[2] Department of Space Science and CSPAR, University of Alabama in Huntsville, Huntsville, AL 35899, USA; gang.li@uah.edu
[3] College of Math and Statistics, Institute of Space Weather, Nanjing University of Information Science and Technology, Nanjing 210044, China
[4] National Center for Space Weather, China Meteorological Administration, Beijing 100081, China
[5] CAS Key Laboratory of Geospace Environment, Department of Geophysics and Planetary Sciences, University of Science & Technology of China, Hefei, Anhui 230026, China
[6] Institute of Space Sciences and School of Space Science and Physics, Shandong University, Weihai, Shandong 264209, China
Received 2014 June 21; accepted 2014 August 31; published 2014 September 15

ABSTRACT

We investigate the eruption and interaction of two coronal mass ejections (CMEs) during the large 2013 May 22 solar energetic particle event using multiple spacecraft observations. Two CMEs, having similar propagation directions, were found to erupt from two nearby active regions (ARs), AR11748 and AR11745, at ∼08:48 UT and ∼13:25 UT, respectively. The second CME was faster than the first CME. Using the graduated cylindrical shell model, we reconstructed the propagation of these two CMEs and found that the leading edge of the second CME caught up with the trailing edge of the first CME at a height of ∼6 solar radii. After about two hours, the leading edges of the two CMEs merged at a height of ∼20 solar radii. Type II solar radio bursts showed strong enhancement during this two hour period. Using the velocity dispersion method, we obtained the solar particle release (SPR) time and the path length for energetic electrons. Further assuming that energetic protons propagated along the same interplanetary magnetic field, we also obtained the SPR time for energetic protons, which were close to that of electrons. These release times agreed with the time when the second CME caught up with the trailing edge of the first CME, indicating that the CME–CME interaction (and shock–CME interaction) plays an important role in the process of particle acceleration in this event.

Key words: acceleration of particles – Sun: coronal mass ejections (CMEs) – Sun: particle emission – Sun: radio radiation

Online-only material: color figures

1. INTRODUCTION

Large solar energetic particle (SEP) events (peak flux intensity >10 pfu in >10 MeV channel, 1 pfu = 1 particle/s sr cm^2) are known to be closely related to coronal mass ejections (CMEs). It is now generally believed that particles are accelerated at shocks driven by fast CMEs in these events (Reames 1999).

Previous works have suggested that shock speed and seed population are two important factors that determine whether a high-intensity SEP event occurs (Kahler 1996; Kahler et al. 2000; Mason et al. 1999, 2000). Kahler (1996) and Kahler et al. (2000) showed that the intensity of SEP events are generally correlated with shock speed, but the scatter was large. Gopalswamy et al. (2002) proposed that CME interaction may be important for SEP production. Later, based on a study of 57 large SEP events, Gopalswamy et al. (2004) found a strong correlation between high particle intensity events and the existence of preceding CMEs within 24 hr of the main CMEs. Li & Zank (2005) suggested that the shock driven by the preceding CMEs can provide both seed particles and enhanced turbulence, leading to an efficient acceleration at the shock driven by the main CME. This work was later refined as the "twin-CME" scenario for the ground level enhancement (GLE) events (Li et al. 2012). In this scenario, the preceding CME and the main CME erupt from the same or nearby source regions close in time. The second shock plows into the downstream of the first shock, experiencing both an enhanced seed particle population due to interchange reconnection that occurs between the closed field lines of the first CME and the open field lines draping the second CME, and an enhanced turbulence due to wave excitation and amplification by streaming protons at the first shock. Consequently, particles are efficiently accelerated at the second shock.

Extending the work of Li et al. (2012), Ding et al. (2013) examined the twin-CME scenario against all large SEP events and fast CMEs with speed >900 km s^{-1} from the western hemisphere in solar cycle 23 and found that most large SEP events agreed with the twin-CME scenario. They also found that the twin-CMEs are more likely to generate large SEP events than single CMEs (Ding et al. 2013, 2014).

Direct observational evidence of enhanced turbulence level and/or seed population as proposed in the twin-CME scenario is difficult to obtain because the acceleration is believed to occur close to the Sun. For example, in a study of all 16 GLE events in solar cycle 23, Gopalswamy et al. (2012b) found that the release heights of these GLEs had a narrow range of 3–4 R_s. Later, Gopalswamy et al. (2013) examined the 2012 May 17 GLE event and found that the release height of energetic particles in this event was ∼2.5 R_s (see their Figure 2). To date, no in situ measurements within <10 R_s exists. Note that the works of Ding et al. (2013, 2014) were based on observations from a single location, therefore the propagation directions of the two CMEs may have large uncertainties. After 2006, CME observations from multiple vantage points became available due to the *STEREO* mission. Indeed, using *STEREO* observations, Shen et al. (2013) suggested that two CMEs, separated by merely

three minutes, erupted in the 2012 May 17 event. Enhanced type II radio bursts, which signify shock–CME interaction (Gopalswamy et al. 2001), were also detected in the 2012 May 17 GLE events. We point out that there are other mechanisms and scenarios in which particles may be efficiently accelerated. For example, if a shock strengthens considerably over a short period of time, efficient particle acceleration can naturally occur.

In this Letter, we study the 2013 May 22 large SEP event. The peak flux intensity detected by the *GOES* satellite of this event was ∼1660 pfu in the >10 MeV channel. NOAA reported a long-duration M5.0 X-ray flare in the AR11745 which was located at (N15,W70). The associated CME had a linear speed of 1466 km s^{-1} in the plane of the sky, as reported by the CDAW database (http://cdaw.gsfc.nasa.gov/CME_list/, Gopalswamy et al. 2009).

Using white light observations, the graduated cylindrical shell (GCS) modeling of the two CMEs, and observations of type II radio bursts, we suggest that the interaction between the shock driven by the second CME and the first CME was the cause of the observed high particle intensity in the 2013 May 22 large SEP event. We discuss how electrons and protons were efficiently accelerated in this event.

2. OBSERVATIONS

We use multiple spacecraft observations in our study. These include energetic particle fluxes detected from the *GOES* and the *STEREO*/HET (Rosenvinge et al. 2008), coronagraph observations from the *SOHO*/LASCO (Brueckner et al. 1995), the *STEREO-A*/*B* (Howard et al. 2008), and radio observation from the Waves instrument and in situ electron observations from the 3DP instrument on board the *Wind* spacecraft (Bougeret et al. 1995; Lin et al. 1995).

2.1. In Situ SEP Observations and the Release Time of Energetic Electrons and Protons

Panel (a) of Figure 1 shows the relative positions of the three spacecraft: *GOES* (Earth), *STEREO-A* (hereafter *STA*), and *STEREO-B* (hereafter *STB*) around 08:20 UT on 2013 May 22. The angular separation between the Earth and *STA* (*STB*) was 141° (137°). The source region of the event was AR11745, which was located at (N15,W70). The event was an eastern event from *STA* and a backside event from *STB*.

Panels (b)–(d) of Figure 1 display the integrated flux intensity time profiles of solar energetic protons in different energy channels as observed by *STA*/HET, *STB*/HET, and *GOES*, respectively. The event was seen in all three spacecraft: the *GOES* spacecraft first detected prompt enhancements in all energy channels around 13:50 UT on May 22. Over six hours later, *STA* detected gradual enhancements in all energy channels around 20:30 UT. The peak flux intensity in *STA* was ∼100 times lower than that observed in *GOES*. After another 23 hr, around 19:00 UT on May 23, the event was seen at *STB*. However, the enhancement was only detected in the lowest energy channel.

Electrons with different energies were observed by the three-dimensional plasma and energetic particles instrument (3DP; Lin et al. 1995) on board the *Wind* spacecraft. This allows one to obtain the solar particle release (SPR) time of these electrons. However, count contamination must be removed when using data from the solid state telescopes (SSTs) of 3DP (Wang et al. 2011; Tan et al. 2013). Here we follow the procedure in Li et al. (2013) to obtain the corrected data.

Panel (e) of Figure 1 shows the corrected electron flux intensity time profiles observed by *Wind*/3DP in five energy channels on 2013 May 22. The arrows mark the beginning of the rising time $t_{\rm rising}$s of these curves from the background. In obtaining these times, we first calculate the average flux ($< f >$) and its standard deviation σ for a 30 minute period (shown as the color bars) prior to the flux peaks; we then identify $t_{\rm rising}$s in the rising phase of each curve from the condition $f(t_{\rm rising}) =< f > +\sigma$. These $t_{\rm rising}$s are plotted as a function of $1/v$ in panel (f).

Using the velocity dispersion analysis (VDA) method (Tylka et al. 2003; Reames 2009; Gopalswamy et al. 2012b), the electron SPR time was obtained to be $13:21 \pm 00:02$ UT and the path length of interplanetary magnetic field (IMF) was 1.12 ± 0.10 AU. Using the eight-hour average solar wind speed centered at the onset time of SEP, which was 444 km s^{-1}, the path length from the Sun to the Earth for a nominal Parker spiral is ∼1.133 AU, comparable to that from the VDA method.

The heavy ion data from ACE/SIS was not of high quality for this event, preventing us from performing an accurate VDA analysis for ions. However, corrected proton data from the *GOES* instrument with a time resolution of five minutes existed.[7] Panels (g)–(i) of Figure 1 show the time intensity profiles for three proton energies of 30.6 MeV, 63.1 MeV, and 165 MeV, respectively. Assuming that the first arriving protons traveled along the same IMF as the electrons, we also estimate the SPR times of protons of different energies, marked by the red arrows in Figure 1(f).[8] For 30.6 MeV protons, it was 13:23 UT, consistent with the SPR time of electrons of 13:21 UT since the time resolution of proton data is five minutes. The SPR times of 63.1 MeV and 165 MeV protons were later. This is conceivable if protons were accelerated diffusively at the shock because the acceleration timescale increases with particle energy (see, e.g., Li et al. 2012).

2.2. Coronagraph Observations

Figure 2 shows the first CME (hereafter CME1) at ∼09:35 UT, which erupted from AR11748 ∼08:48 UT in the view of LASCO C2. The CME was well observed in all three spacecraft (*STB*, *SOHO*, and *STA*). The top three panels of Figure 2 are base difference images from *STB*/SECCHI COR1, *SOHO*/LASCO C2, and *STA*/SECCHI COR1, respectively. In the lower panels of Figure 2, we overlap the flux ropes (green grids) as modeled by the GCS model at the time of ∼09:35 UT. The GCS model contains six free parameters to describe a CME's shape in three-dimensional space. These parameters are longitude ϕ, latitude θ, height of the leading edge h, aspect ratio κ, tilt angle γ with respect to the equator, and half angular width δ between the two flux rope legs (Thernisien et al. 2006, 2009, 2011).

About 4.5 hr later, at ∼13:25 UT, another fast CME (hereafter CME2) erupted from AR11745 in the view of LASCO C2. This is shown in Figure 3. In the lower panels of Figure 3, the flux rope for CME2 is shown by the red grids. We also overlay the modeled flux rope of CME1 by the green grids. The propagation directions of CME1 and CME2 were similar.

The parameters of CME1 and CME2 as modeled by the GCS model at different times are shown in Table 1. The first column is the observation time; Column 2 (3) is the longitude (latitude)

[7] See http://satdat.ngdc.noaa.gov/sem/goes/data/new_avg/2013/05/goes15/csv/.

[8] For protons, we use a six hour period (shown by the horizontal thick lines) to calculate the average flux $< f >$ and its standard deviation σ.

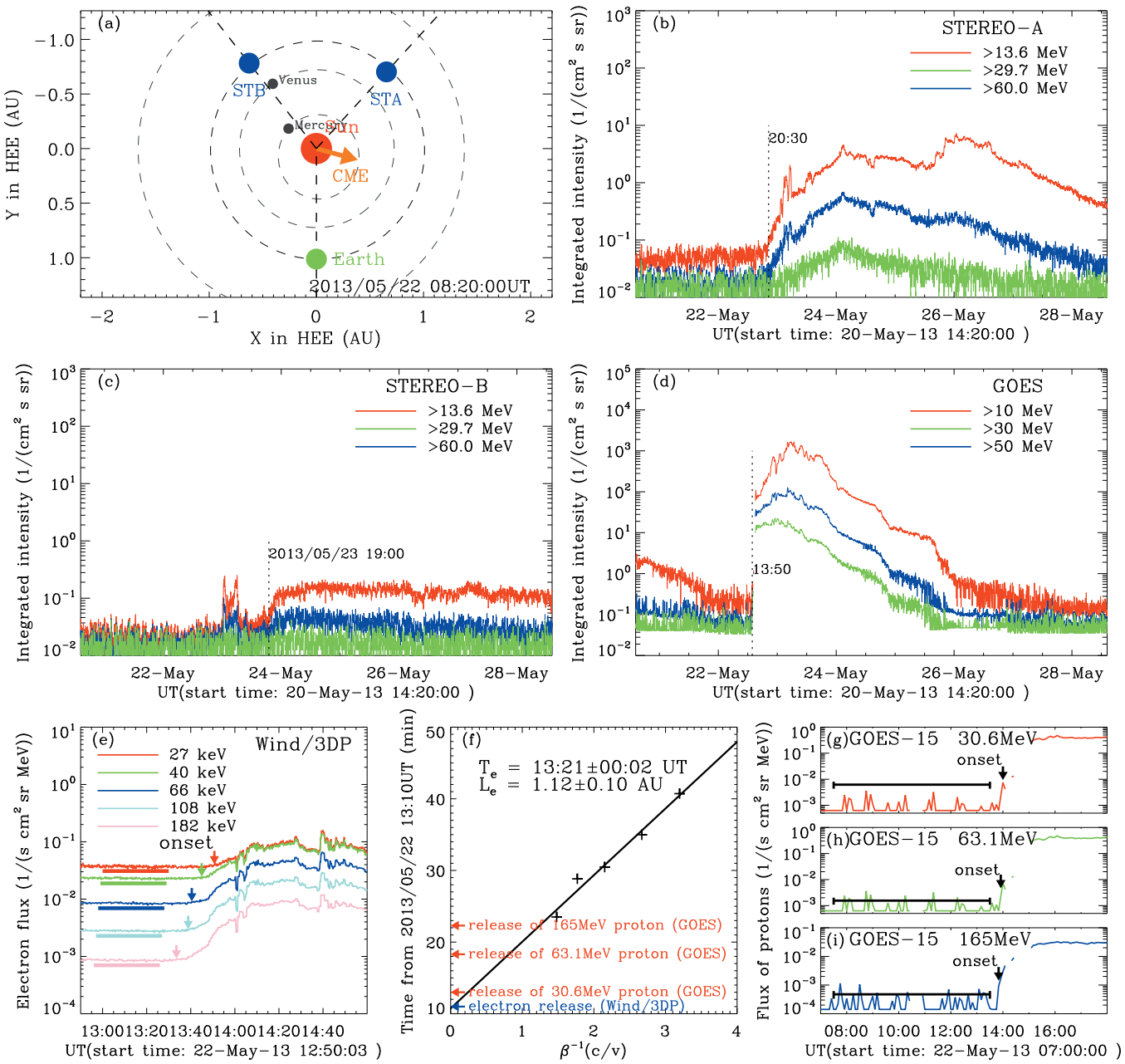

Figure 1. (a) Positions of the Earth, *STA*, and *STB*. The angle between the Earth and *STA* (*STB*) is 141° (137°). (b)–(d) Ion fluxes seen at *GOES*, *STA*, and *STB*. The vertical dashed lines indicate the onset times of SEP detected by different spacecraft. (e) Energetic electron fluxes in different energy channels on board the *Wind*/3DP instrument. (f) The electron SPR and path length as obtained from the VDA method. (g)–(i) Time intensity profiles and onset times of energetic protons from the *GOES-15* spacecraft.

(A color version of this figure is available in the online journal.)

of the CME propagation direction; Column 4 is the height of the leading edge of the flux rope; Column 5 is the half angular width of the flux rope; Column 6 is the tilt angle; Column 7 is the aspect ratio; Column 8 is the radius of the flux rope at the leading edge; and Columns 9 and 10 are the angular widths of the flux rope as viewed from the front and the side, respectively. The fitting results show that the two CMEs had a latitude difference of ∼16° and nearly the same tilt angles with respect to the equator. Because the flare and flux rope locations were different (see Table 2 of Gopalswamy et al. 2014), the real latitude difference may be smaller. Since CME2 moved faster than CME1, it caught up with and interacted with CME1. The height of the two CMEs at different times are plot in panel (a) of Figure 4. The black squares denote the leading edge of CME1, and the blue triangles denote the leading edge of CME2. From the linear fittings of their leading edge heights, we can obtain the speeds of the two CMEs, which were 519 ± 7 km s^{-1} for CME1 and 1439 ± 22 km s^{-1} for CME2. The green circles denote the trailing edge of the flux rope of CME1, obtained by subtracting the diameter ($2\,r_a$) of the flux rope from the leading edge. Using data from Table 1, the peak speed of CME2 was ∼1800 km s^{-1} and occurred between 13:54 UT and 14:24 UT. This is higher than the plane of the sky speed 1466 obtained from CDAW and is comparable to the estimate of Gopalswamy et al. (2014), who also used the GCS model and obtained a peak speed of 1881 km s^{-1} for this event.

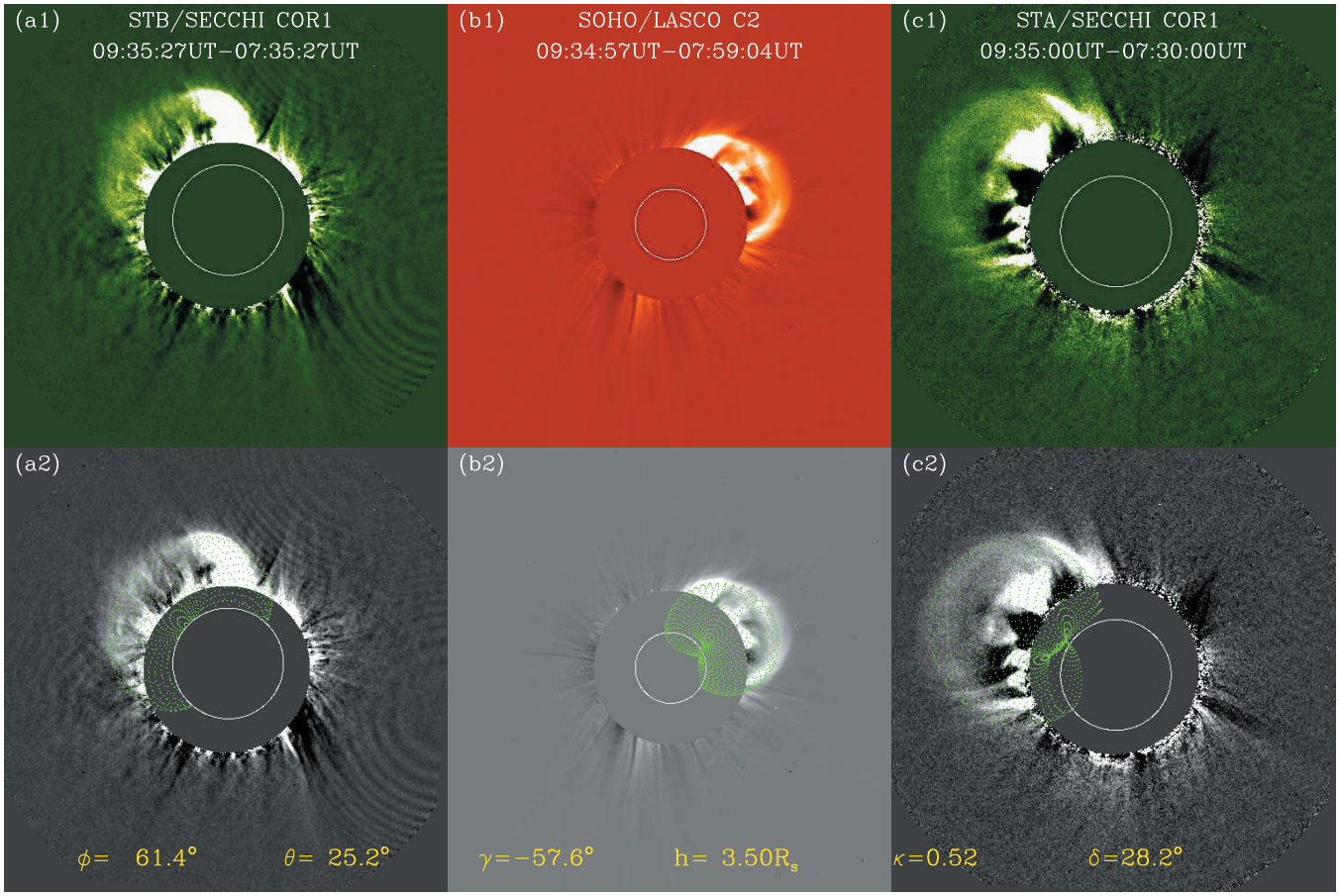

Figure 2. Top: coronagraph observations near 9:35 UT on 2013 May 22 from *STB*, *SOHO*, and *STA*. Bottom: the GCS modeling results of CME1 at the same times as in the top panels.

(A color version of this figure is available in the online journal.)

Table 1
The Results of GCS Model Fitting for CME1 and CME2

Obs. time	Lon. (ϕ)	Lat. (θ)	Height (h)	δ	γ	κ	r_a	WD_{face}	WD_{edge}
				CME1					
2013 May 22 08:47:30	71.45	24.00	2.60	27.67	−63.20	0.13	0.30	70.28	14.94
2013 May 22 09:10:00	59.20	20.68	3.00	27.67	−66.52	0.33	0.74	93.48	38.13
2013 May 22 09:35:00	61.35	25.20	3.50	28.20	−57.60	0.52	1.20	119.06	62.66
2013 May 22 10:00:00	64.80	30.70	4.57	38.30	−65.40	0.35	1.18	117.57	40.97
2013 May 22 10:24:00	73.73	29.63	6.07	59.81	−73.23	0.40	1.74	166.84	47.21
2013 May 22 10:54:00	74.01	29.63	7.57	59.81	−73.23	0.40	2.17	166.84	47.21
2013 May 22 11:39:00	74.40	29.60	9.36	37.17	−73.20	0.40	2.67	121.50	47.16
2013 May 22 12:24:00	74.84	29.63	11.50	31.30	−73.23	0.40	3.29	109.82	47.21
2013 May 22 12:54:00	75.09	29.60	12.71	31.30	−73.20	0.40	3.63	109.76	47.16
2013 May 22 13:54:00	75.62	31.86	15.86	22.40	−73.20	0.40	4.53	91.96	47.16
2013 May 22 14:24:00	75.90	31.86	16.64	22.40	−73.20	0.40	4.76	91.96	47.16
2013 May 22 14:39:00	76.03	31.86	17.64	22.40	−73.20	0.40	5.04	91.96	47.16
				CME2					
2013 May 22 13:25:00	74.85	6.10	4.07	30.00	−73.80	0.34	1.03	99.75	39.75
2013 May 22 13:39:00	71.50	12.30	6.43	69.04	−59.25	0.43	1.92	188.38	50.31
2013 May 22 13:54:00	77.05	16.21	7.93	80.78	−59.30	0.39	2.24	208.00	46.45
2013 May 22 14:24:00	69.15	17.90	11.64	67.10	−59.30	0.45	3.61	187.69	53.49
2013 May 22 14:39:00	71.45	13.40	13.64	57.30	−73.20	0.52	4.67	177.31	62.71
2013 May 22 14:54:00	71.25	13.40	15.43	46.40	−73.20	0.56	5.54	160.91	68.11
2013 May 22 15:24:00	71.85	13.40	19.07	57.30	−73.20	0.56	6.85	182.71	68.11

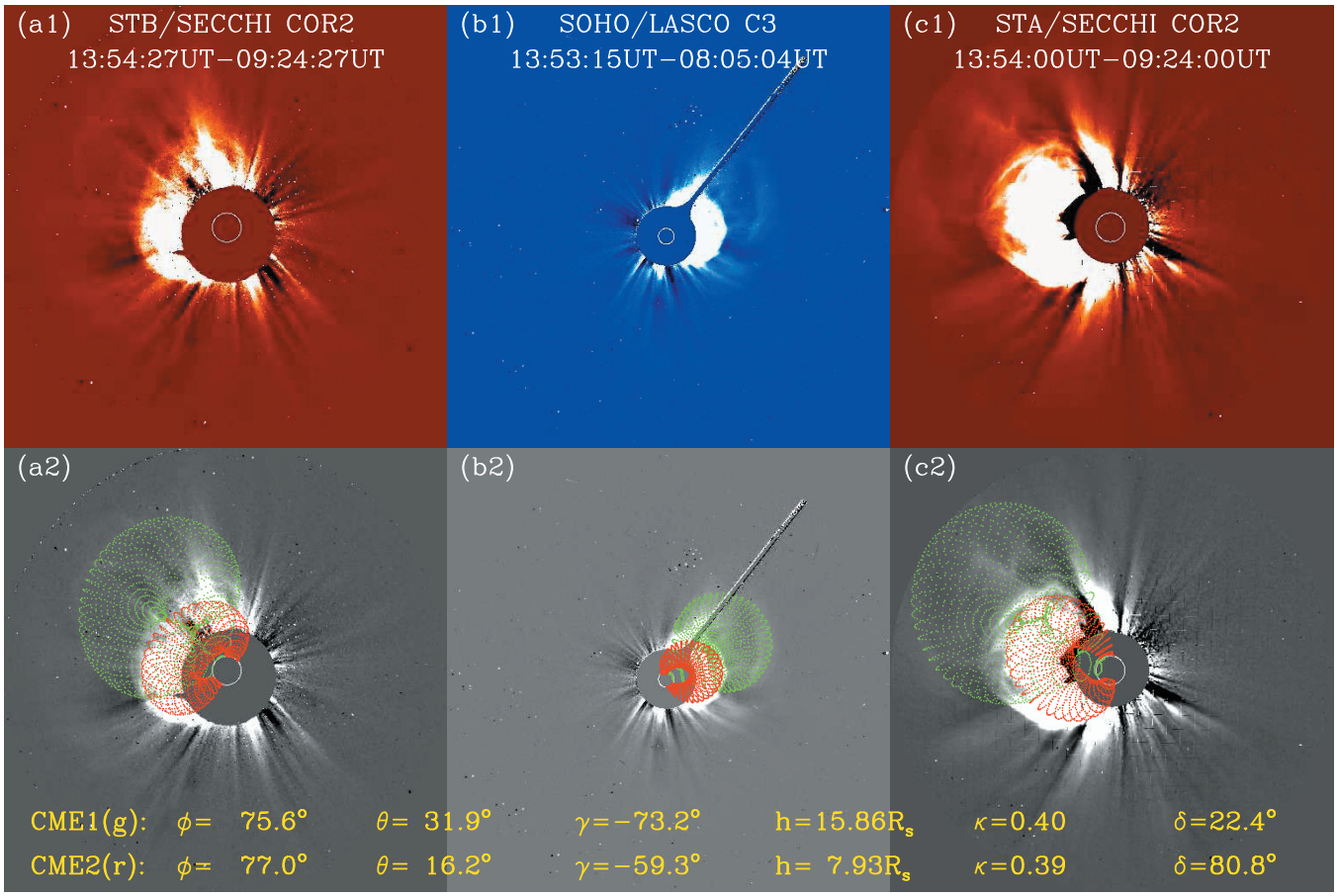

Figure 3. Top: coronagraph observations near 13:54 UT on 2013 May 22 from *STB*, *SOHO*, and *STA*. Bottom: the GCS modeling results of CME1 (green) and CME2 (red) at the same times as in the top panels.

(A color version of this figure is available in the online journal.)

Fitting CME1's trailing edge and CME2's leading edge as two straight lines, we obtain the intersection point, labeled "Q" in panel (a) of Figure 4. Point "Q" indicates when and where the leading edge of CME2 began to overtake the tailing edge of the flux rope of CME1. The time of "Q" was 13:32 ± 00:09 UT and the corresponding height was 6.4 ± 0.3 R_s. Similarly, we obtain point "P," which was the point when the leading edges of the two CMEs merged together. The time was 15:21 ± 00:14 UT and the height was 19.8 ± 0.7 R_s. The electron and 30.6 MeV proton onset times are also marked in panel (a) of Figure 4 by the red and cyan arrows. We see that the SPR time for electrons and the 30.6 MeV protons were close to that of point "Q."

2.3. Radio Observations

Panel (b) of Figure 4 shows the radio observation in the frequency range of 0.02–14 MHz as detected by *Wind*/Waves. A type III radio burst with 14 MHz appeared around ∼13:00 UT. As shown in panel (c), this time was very close to the peak of the time derivative of the soft X-ray flux (shown as the blue dots), a proxy for hard X-ray emissions. This coincidence suggests that this type III radio burst was caused by energetic electrons accelerated at the flare site. Note that none of these three spacecraft observed noticeable energetic electrons near the type III radio burst. This is not surprising since the longitudinal spreading of the flare was small, so there was no magnetic connection between the flare site and any spacecraft.

Also shown in panel (b) of Figure 4 is a type II radio burst, caused by electrons that were accelerated at the CME-driven shock. While the beginning portion of the type II burst was not continuous, the onset time can be identified as 13:23 UT. This was very close to the electron SPR time obtained from the VDA method, indicating that energetic electrons that generated the type II radio bursts also propagated along the Parker field lines that were magnetically connected to the *Wind* spacecraft. This is conceivable since these electrons were accelerated at the shock front, which had a much larger longitudinal extension than the flare. The type II radio burst became weaker after 15:30 UT and a clear change of the frequency drift rate occurred around 16:00 UT. Between 13:23 UT and 15:30 UT, the radio signal resembled those of shock–CME interaction as examined in Gopalswamy et al. (2001).

The first CME was slow and there was no type II radio bursts associated with the first CME. Consequently, it might not drive a shock and there would be no seed particles produced or enhanced turbulence. Of course, not all SEP events are associated with type II radio bursts. Thus, it is possible that there was a radio-quiet shock associated with the first CME.

Our event is to be compared with the 2002 May 22 SEP event and the 2005 January 17 events. Gopalswamy & Yashiro (2013), in a study of flare emission obscuration by an eruptive prominence, noted that two eruptions occurred in the 2002 May 22 SEP event: the first a partial halo CME with a speed of 1246 km s^{-1} and the second a full halo CME with a speed

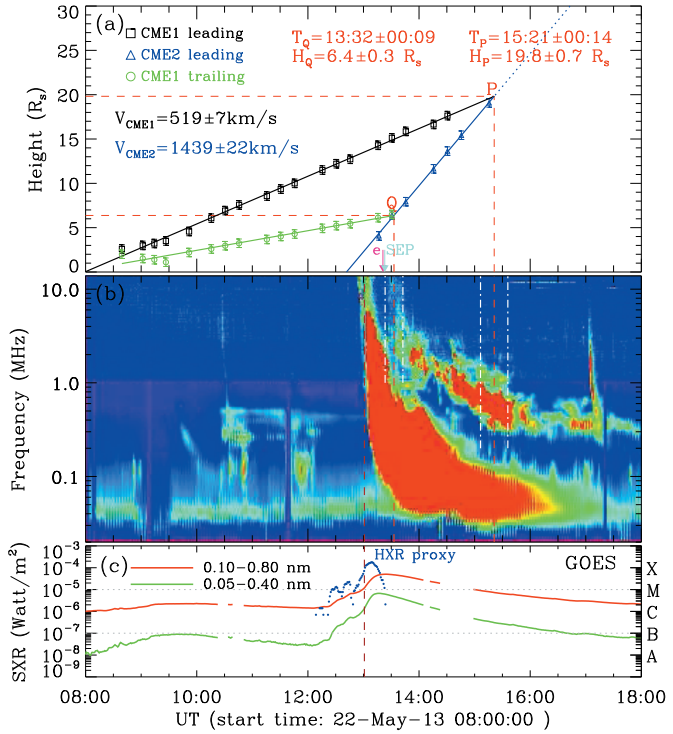

Figure 4. (a) Heights of the leading edge (black) of CME1, the trailing edge (green) of CME1, and the leading edge (blue) of CME2, as a function of time, from the fitting results of GCS model. The point "Q" denotes the time when the second CME caught the flux rope of the first CME. The point "P" denotes the time when the leading edges of the two CMEs merged. The two red dashed lines indicate the times for "Q" and "P," with the braking white dot–dashed lines showing the uncertainties. (b) Radio observations from *Wind*/Waves. Both type III and type II radio bursts can be seen. The type II emission between "Q" and "P" resembles that of shock–CME interaction as investigated in (Gopalswamy et al. 2001). (c) The soft X-ray fluxes detected by *GOES* for two channels. The blue dots are the derivative of the 0.10–0.80 nm channel, as a proxy for hard X-rays. Note that times for electromagnetic observations have been subtracted by 8.3 minutes.

(A color version of this figure is available in the online journal.)

of 1557 km s^{-1}. The first CME in that event was faster than our event and the likelihood of generating a shock was higher. However, although both CMEs were fast, only the second CME produced an interplanetary type II radio burst. In the case of the 2005 January 17 events, two fast CMEs and two type II bursts were identified (see Figure 3 of Gopalswamy et al. 2012a), providing a clear case for seed particles.

3. DISCUSSION AND CONCLUSION

It is interesting to note that the SPR time of electrons and 30 MeV protons in this event were consistent with the beginning of the type II radio burst. These times were slightly earlier than the time of point "Q" when the leading edge of CME2 caught up with the trailing edge of CME1. They may correspond to the time when the shock driven by CME2 interacts with the trailing edge of CME1.

Assuming that this event agreed with the twin-CME scenario, then, as anticipated by the twin-CME scenario, efficient ion acceleration was achieved through the enhanced seed population and enhanced turbulence level at the shock driven by CME2.

The enhanced turbulence was mostly in the form of Alfvén waves and was generated by streaming protons upstream the shock driven by CME1. It was further amplified upon transmitting through the shock. These waves, however, did not resonate with electrons. So, why were electrons also efficiently accelerated when the shock driven by CME2 caught up CME1?

To see this, we note that the flux rope of CME1 had its two legs rooted on the solar surface and therefore had a closed magnetic field topology. When the shock driven by CME2 caught up with CME1, the field lines of the flux rope of CME1 intersected with the shock at multiple places. Electrons propagating along these field lines either crossed the shock or were reflected at these points, and in both cases were accelerated. This is analogous to that shown in Figure 4 of Shen et al. (2008), where a shock driven by a CME plows into the magnetic cloud of a previous CME. Such a magnetic field configuration presumably occurs often when CME–CME interact and can lead to complex ejecta that are often observed (Farrugia & Berdichevsky 2004; Dasso et al. 2009). A similar configuration has also been studied by Kong et al. (2014) in examining electron acceleration in a streamer-shock interaction system. There were also open field lines that draped the first CME. These open field lines threaded and mixed with the closed field lines of the flux rope of CME1. Electrons accelerated in the closed field lines can access these open field lines and escape from the shock through, e.g., curvature drift. These escaped energetic electrons led to the type II radio bursts that were observed by *Wind*/Waves and they themselves were also observed in situ by *Wind*/3DP.

In summary, we have examined the 2013 May 22 large SEP event from in situ particle measurements, remote-sensing coronagraph observations, and type-II and III solar radio bursts. Our study suggests that both electrons and protons (ions) were efficiently accelerated in the 2013 May 22 event. The acceleration of electrons and >30 MeV protons occurred when the shock driven by the second CME interacted with the first CME. This event illustrates that shock–CME interaction can play an important role in generating large SEP events.

We are grateful to the *SOHO*, *STEREO*, *GOES*, and *Wind* spacecraft for making their data available online. We acknowledge the usage of the online CDAW catalog. This work is supported at UAH by NSF grants ATM-0847719 and AGS-1135432; at NUIST by NSFC (Nos. 41304150, 41174165, 10847147), NSF for colleges and universities in Jiangsu (12KJB170008); Jiangsu Government Scholarship for Overseas Studies (JS2012-105) for B.G.; at CMA by NSFC (41074132, 41274193).

REFERENCES

Bougeret, J. L., Kaiser, M. L., Kellogg, P. J., et al. 1995, SSRv, 71, 231
Brueckner, G. E., Howard, R. A., Koomen, M. J., et al. 1995, SoPh, 162, 357
Dasso, S., Mandrini, C. H., Schmieder, B., et al. 2009, JGR, 114, A02109
Ding, L., Jiang, Y., Zhao, L., & Li, G. 2013, ApJ, 763, 30
Ding, L.-G., Li, G., Dong, L.-H., et al. 2014, JGR, 119, 1463
Farrugia, C. D., & Berdichevsky, 2004, AnGeo, 22, 3679
Gopalswamy, N., MäKelä, P., Akiyama, S., et al. 2012a, JGR, 117, A08106
Gopalswamy, N., Xie, H., Akiyama, S., MäKelä, P., & Yashiro, S. 2014, EP&S, in press (arXiv:1408.3617)
Gopalswamy, N., Xie, H., Akiyama, S., et al. 2013, ApJL, 765, L30
Gopalswamy, N., Xie, H., Yashiro, S., et al. 2012b, SSRv, 171, 23
Gopalswamy, N., & Yashiro, S. 2013, PASJ, 65, S11
Gopalswamy, N., Yashiro, S., Kaiser, M. L., et al. 2001, ApJL, 548, L91
Gopalswamy, N., Yashiro, S., & Krucker, S. 2004, JGR, 109, 1
Gopalswamy, N., Yashiro, S., Michalek, G., et al. 2002, ApJL, 572, L103
Gopalswamy, N., Yashiro, S., Michalek, G., et al. 2009, EM&P, 104, 295
Howard, R. A., Moses, J. D., Vourlidas, A., et al. 2008, SSRv, 136, 67
Kahler, S. W. 1996, in AIP Conf. Proc. 374, High Energy Solar Physics, ed. R. Ramaty, N. Mandzhavidze, & X.-M. Hua (Melville, NY: AIP), 61

Kahler, S. W., Reames, D. V., & Burkepile, J. T. 2000, in ASP Conf. Ser. 206, High Energy Solar Physics Workshop—Anticipating HESSI, ed. R. Ramaty & N. Mandzhavidze (San Francisco, CA: ASP), 468
Kong, X., Chen, Y., Guo, F., et al. 2014, ApJ, submitted
Li, C., Firoz, K. A., Sun, L., & Miroshnichenko, L. 2013, ApJ, 770, 34
Li, G., Moore, R., Mewaldt, R. A., Zhao, L., & Labrador, A. W. 2012, SSRv, 171, 141
Li, G., & Zank. 2005, in Proc. of 29th International Cosmic Ray Conference, Vol. 1, ed. B. Sripathi Acharya et al. (Mumbai: Tata Institute of Fundamental Research), 173
Lin, R., Anderson, K., Ashford, S., et al. 1995, SSRv, 71, 125
Mason, G. M., Dwyer, J. R., & Mazur, J. E. 2000, ApJL, 545, L157
Mason, G. M., Mazur, J. E., & Dwyer, J. R. 1999, ApJL, 525, L133
Reames, D. V. 1999, SSRv, 90, 413
Reames, D. V. 2009, ApJ, 706, 844
Shen, C., Li, G., Kong, X., et al. 2013, ApJ, 763, 114
Shen, C., Wang, Y., Ye, P., & Wang, S. 2008, SoPh, 252, 409
Tan, L. C., Malandraki, O. E., Reames, D. V., et al. 2013, ApJ, 768, 68
Thernisien, A., Howard, R. A., & Vourlidas, A. 2006, ApJ, 652, 763
Thernisien, A., Vourlidas, A., & Howard, R. A. 2009, SoPh, 256, 111
Thernisien, A., Vourlidas, A., & Howard, R. A. 2011, JASTP, 73, 1156
Tylka, A. J., Cohen, C. M. S., Dietrich, W. F., et al. 2003, in Proc. of 28th International Cosmic Ray Conference, ed. T. Kajita et al. (Tokyo: Universal Academy Press), 3305
von Rosenvinge, T., Reames, D., Baker, R., et al. 2008, SSRv, 136, 391
Wang, L., Lin, R., & Krucker, S. 2011, ApJ, 727, 121